Nuclear Materials and Energy 9 (2016) 338–341

Contents lists available at ScienceDirect

Nuclear Materials and Energy

journal homepage: www.elsevier.com/locate/nme

Grain boundary sliding associated with low strain rate at 1000 °C in recrystallized ODS ferritic steel

R. Kamikawa[a,*], S. Ukai[a], N. Oono[a], T. Kaito[b], T. Torimaru[c], A. Kimura[d], S. Hayashi[e], H. Masuda[f], E. Sato[f]

[a] Faculty of Engineering, Hokkaido University, Sapporo 060-8628, Japan
[b] Japan Atomic Energy Agency, Ibaraki 311-1393, Japan
[c] Nippon Nuclear Fuel Development Co. LTD., Ibaraki 311-1313, Japan
[d] Advanced Energy Institute, Kyoto University, Uji 611-0011, Japan
[e] Tokyo Institute of Technology, Ohokayama 152-8552, Japan
[f] Institute of Space and Astronautical Science, JAXA, Sagamihara 252-5210, Japan

ARTICLE INFO

Article history:
Received 16 November 2015
Revised 2 August 2016
Accepted 4 August 2016
Available online 24 August 2016

Keywords:
ODS
Grain boundary sliding
Dislocation creep
Diffusional creep

ABSTRACT

The high-temperature deformation process of the recrystallized 16CrODS ferritic steel was investigated at 1000 °C for the stress loading perpendicular to the elongated grain structure. The strain rate was varied in the range from 1.0×10^{-2} to 1.0×10^{-5} s^{-1}. At the strain rate over 1.0×10^{-4} s^{-1}, deformation is dominated by the conventional dislocation creep. Decreasing strain rate from 1.0×10^{-4} s^{-1}, grain boundary sliding becomes prominent. Accommodation process for the localized stress induced by grain boundary sliding could be dislocation creep at 1.0×10^{-4} s^{-1}, and by diffusional creep at 1.0×10^{-5} s^{-1} or less. These were verified through the observation of void formation and localized strain accumulation by KAM map.

1. Introduction

Oxide dispersion strengthened (ODS) ferritic steels are expected as the candidate materials for the advanced fusion blanket as well as Generation IV fast reactors claddings [1–3], since they have superior high-temperature strength and radiation resistance. Their high-temperature mechanical properties have been mainly evaluated up to around 800 °C, corresponding to the steady state operational condition. However, the temperature of the reactor materials may occasionally rise beyond steady state condition, and an understanding of the deformation mechanism at such higher temperature is substantially limited. In general, grain boundary sliding (GBS) becomes more prominent at the elevated temperatures, and accommodation process for the stress induced by GBS could be affected by the strain rate [4]. In this study, deformation process of the ODS ferritic steels was investigated at 1000 °C, varying with strain rates.

2. Material and methods

16CrODS ferritic steel was produced by mechanical alloying. The Fe-base atomized master powder containing Cr, Al and Ti were mechanically alloyed (MAed) together with Y_2O_3 powder for 48 h by attrition type ball mill under argon atmosphere. MAed powders were consolidated by hot-extrusion at 1150 °C, then annealed at 1150 °C for 1 h. The hot-extruded bar was cold-rolled with 85% reduction in parallel to the hot-extruded direction, and followed by annealing at 900 °C to make recrystallized grain structure. Yttria was forcibly decomposed during MA, and was finely dispersed as Y_2O_3 particles by internal oxidation at the hot-extrusion process. The final chemical composition is Fe–16.73Cr–6.28Al–0.49Ti–0.033C–0.47Y_2O_3–0.12Ex.O (wt%), which is result of chemical analyses. The tensile specimens were prepared in a gauge length of 5 mm, width of 1.2 mm, thickness of 0.5 mm, along with a direction perpendicular to the cold-rolled and elongated grain structure. Tensile test was carried out at 1000 °C under argon gas atmosphere. The strain rate ranges 1×10^{-5}–1×10^{-2} s^{-1}. After tensile test, grain structure was observed by SEM/EBSD. Kernel Average Misorientarion (KAM) was analyzed with its step size of 1 μm to estimate a strain accumulated inside grain interior and grain boundaries.

* Corresponding author.
E-mail address: kamikawa-ryoma@eis.hokudai.ac.jp (R. Kamikawa).

http://dx.doi.org/10.1016/j.nme.2016.08.006

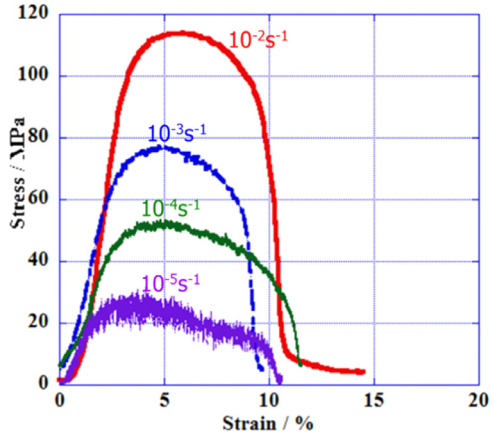

Fig. 1. Engineering stress–strain curves at 1000 °C and four levels of strain rates; 1.0×10^{-2}, 1.0×10^{-3}, 1.0×10^{-4}, 1.0×10^{-5} s^{-1}.

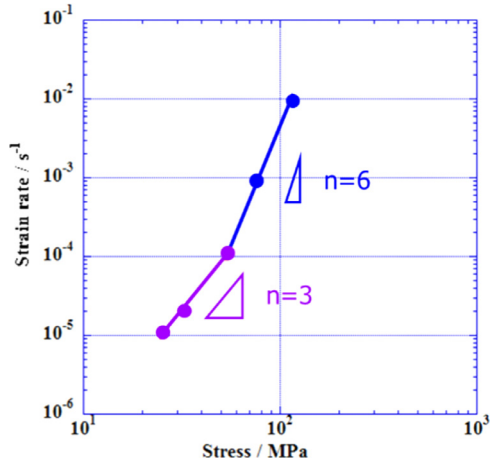

Fig. 2. Double logarithm plots of strain rate versus stress: n for creep exponent at 1000 °C.

3. Results

3.1. Tensile tests

Fig. 1 shows the engineering stress–strain curves obtained by the tensile tests. The ultimate tensile stress (UTS) decreases with decreasing the strain rate from 10^{-2} to 10^{-5} s^{-1}. Total elongations are almost constant around 10%. Fig. 2 represents a double logarithm plot of stress–strain rate. The relation between stress σ and strain rate $\dot{\varepsilon}$ is described by $\dot{\varepsilon} = A\sigma^n$, where n is stress exponent. The plot can be divided into two regions. The stress exponent (n) is 6 at the strain rate of 1×10^{-2}–1×10^{-4} s^{-1}, suggesting that the dominant deformation mode is dislocation creep. Decreasing strain rate to 1×10^{-5} from 1×10^{-4} s^{-1}, n-value gradually decreases to 3 or less. It is well known that the deformation mode by GBS takes $n = 2$ [4]; therefore, rate-limiting process at strain rate of 1×10^{-5} s^{-1} or less could be attributed to the GBS.

3.2. Microstructural observation

Fig. 3 shows SEM images of tensile specimens after tensile tests. Gauge parts of the tensile specimens, where stress was loaded, contain small voids, whereas shoulder parts of tensile specimens without loading contain no void. This means that voids were formed during deformation. It is obvious that void size becomes larger as the stain rate decreases; i.e. the voids size is around 3–5 μm at the strain rate of 1×10^{-3}–1×10^{-4} s^{-1}, and it increases to around 10 μm at 1×10^{-5} s^{-1}.

Fig. 4 compares KAM maps of shoulder and gauge parts after tensile test at the strain rate of 1×10^{-3}, 1×10^{-4} and 1×10^{-5} s^{-1}. At the strain rate of 1×10^{-3} s^{-1}, shown in Fig. 4(a) and (b), gauge part has stronger KAM contrast by 0.23 degree than shoulder part. At the strain rate of 1×10^{-4} s^{-1}, as shown in Fig. 4(c) and (d), gauge part has KAM value of 0.15 degree higher than shoulder part. These contrasts are the result of intra-grain deformation by dislocation gliding, suggesting that deformation at 1×10^{-3} and 1×10^{-4} s^{-1} is dominated by the dislocation creep mode. On the contrary, from Fig. 4(e), (f) KAM value of gauge part is only 0.02 degree higher than shoulder part at the strain rate of 1×10^{-5} s^{-1}. Therefore, dislocation creep is not dominant at 1×10^{-5} s^{-1}. The magnified views of specimen at 1×10^{-5} s^{-1} is represented in Fig. 5, where voids are located at grain boundaries and strong KAM contrast is localized at near voids, which implies that stress concentration induced by GBS gives vacancy diffusional flow, and leads to the void formation.

Fig. 6 shows the double logarithm plots with area ratio of void and KAM value versus strain rate. Area ratio of void could be resulted from the accumulation of the vacancies to relax the stress concentration, and KAM value corresponds to the amount of stress concentration. At lower strain rate of 1×10^{-5} s^{-1}, KAM value is especially low and area ratio of voids is high. This trend is evidence of the deformation mode induced by GBS and vacancy flow as the accommodation process.

4. Discussion

Mass transfer via vacancy diffusional flow [4-6] and dislocation movement [7] are considered as the relaxation processes for the stress concentration induced by GBS. At the strain rate of 1.0×10^{-4} s^{-1}, relatively strong KAM contrast is generated, but it is weaker than that of 1.0×10^{-3} s^{-1} where the deformation proceeds through the typical dislocation creep mode because of the stress exponent, n, is equal to 6.0, as indicated in Fig. 4. In addition, void is hardly observed in the case of 1.0×10^{-4} s^{-1}. Therefore, the dominant deformation mode at 1.0×10^{-4} s^{-1} is considered to be attributed to GBS and dislocation creep as the accommodation process to relieve the stress concentration. Masuda et al. [8] have recently proposed the core–mantle deformation model at this strain rate of 1.0×10^{-4} s^{-1} based on Gifkins work [9]. They have observed the regions with much higher dislocation densities in narrow areas near the grain boundaries (mantles) than the grain interiors (cores). The low-angle boundaries have been also found to emerge at the core–mantle boundaries via sloping of dislocations within the mantle region.

At decreasing strain rate of 1.0×10^{-5} s^{-1}, KAM contrast becomes weaker and there are many voids at the grain boundaries as shown in Figs. 4 and 5. Grain switching event and grain boundary sliding have been previously observed at the similar strain rate condition [10–12]. These results suggest that vacancy diffusion becomes more active at around grain boundaries. Based on above results, the high temperature deformation of ODS ferritic steels is considered to proceed in a following process at slow strain rate of less than 1.0×10^{-5} s^{-1} and at around 1000 °C. At first, GBS occurs, but it cannot continue by a restriction from the adjacent grains, where the stress is locally concentrated. The stress gradient produces a gradient of vacancy concentration, and thus vacancy flow induces diffusional creep, according to the Nabarro–Hering model [13] or grain boundary diffusion by the Coble model [14]. As a result of vacancy flows and concomitant void formation, a mismatch of grain boundaries is accommodated and the stress concentration can be relieved; consequently deformation continues through GBS and diffusional creep.

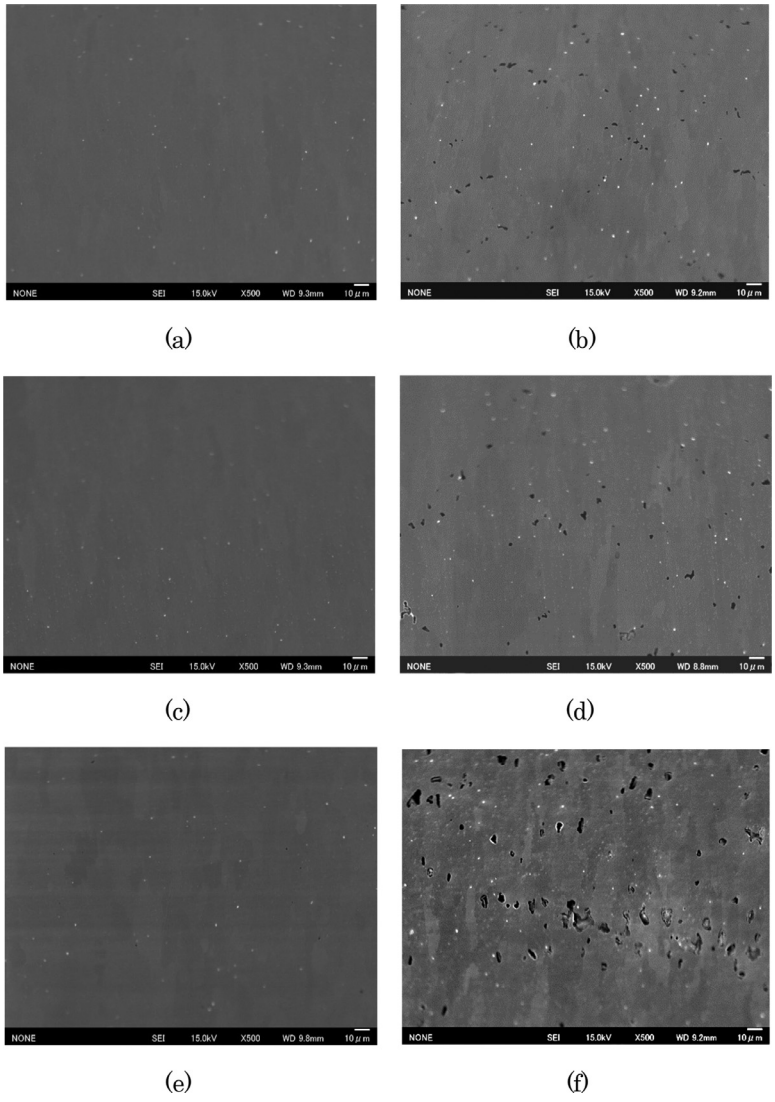

Fig. 3. SEM images of tensile specimens: 1.0×10^{-3} s^{-1} at (a) shoulder part (b) gauge part, 1.0×10^{-4} s^{-1} at (c) shoulder part (d) gauge part, and 1.0×10^{-5} s^{-1} at (e) shoulder part (f) gauge part.

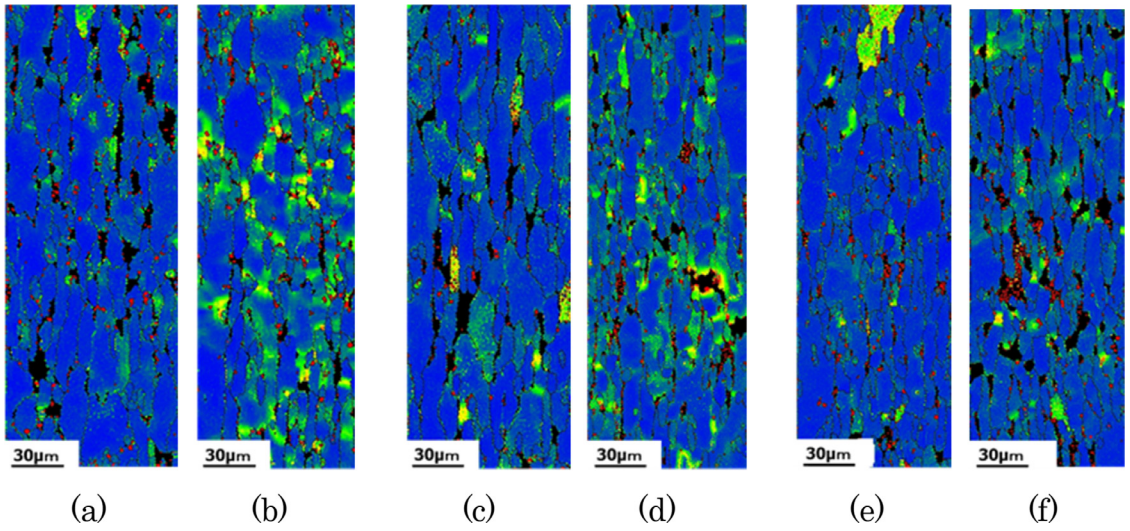

Fig. 4. KAM maps after tensile test: strain rate of 1.0×10^{-3} s^{-1} at (a) shoulder part (b) gauge part, 1.0×10^{-4} s^{-1} at (c) shoulder part (d) gauge part, 1.0×10^{-5} s^{-1} at (e) shoulder part (f) gauge part. (b) and (d) have strong KAM contrast, but (f) shows weak KAM contrast.

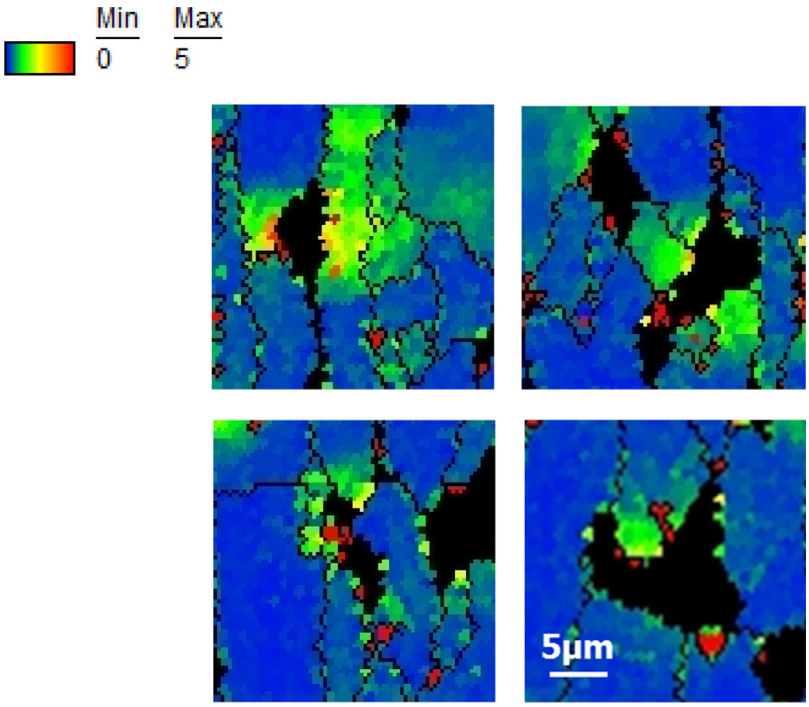

Fig. 5. Magnified views of Fig. 4(f); voids are accumulated at grain boundaries, strong KAM contrast is located near voids.

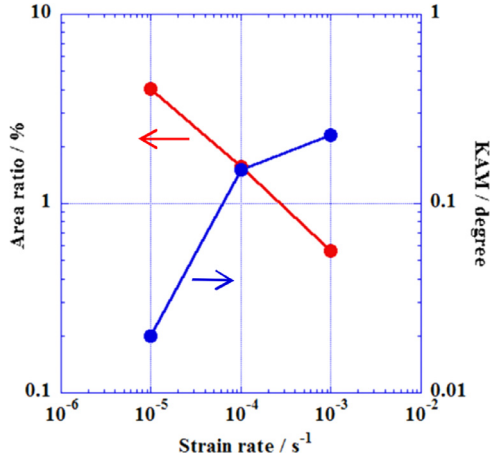

Fig. 6. Double logarithm plots for area ratio of void and KAM value versus strain rate.

5. Conclusion

The high-temperature deformation process of the recrystallized 16CrODS ferritic steel was investigated at 1000 °C with varying strain rates. Tensile stress was loaded along direction perpendicular to the elongated grain structure. At the strain rate of $1.0 \times 10^{-4}\,s^{-1}$, dominant deformation is attributed to GBS and dislocation creep as the stress accommodation process. Decreasing strain rate to $1.0 \times 10^{-5}\,s^{-1}$ or less, stress accommodation process could be changed to the diffusional creep, which was verified through the observation of void formation and localized strain accumulation. Conventional dislocation creep is attributed to the deformation at the strain rate over $1.0 \times 10^{-4}\,s^{-1}$.

Acknowledgement

This study is the result of "R&D of ODS ferritic steel fuel cladding for maintaining fuel integrity at the high temperature accident condition" entrusted to Hokkaido University by the Ministry of Education, Culture, Sports, Science and Technology of Japan (MEXT).

References

[1] R.L. Klueh, P.J. Maziasz, I.S. Kim, L. Heatherly, D.T. Hoelzer, N. Hashimoto, E.A. Kenik, K. Miyahara, J. Nucl. Mater. (2002) 773 307–311.
[2] G.R. Odette, M.J. Alinger, B.D. Wirth, Annu. Rev. Mater. Res. 38 (2008) 471–503.
[3] S. Ukai, M. Fujiwara, J. Nucl. Mater. (2002) 749–757 307–311.
[4] T.G. Langdon, Mater. Sci. Eng. A137 (1991) 1–11.
[5] M.F. Ashby, R.A. Verrall, Acta Metall. 21 (1973) 149.
[6] M.F. Ashby, Surf. Sci. 31 (1972) 498.
[7] A. Ball, M.M. Hutchison, Met. Sci. J. 3 (1969) 1.
[8] H. Masuda, H. Tobe, E. Sato, Y. Sugino, S. Ukai, Philos. Mag. Lett. (2015). http://dx.doi.org/10.1080/09500839.2015.1067732.
[9] R.C. Gifkins, Metall. Trans. A 7A (1976) 1225.
[10] S. Taniguchi, N. Kawai, E. Sato, Mater. Sci. Forum 735 (2013) 79.
[11] H. Masuda, S. Taniguchi, E. Sato, Y. Sugino, S. Ukai, Mater. Trans. 55 (10) (2014) 1599–1605.
[12] Y. Sugino, S. Ukai, N. Oono, S. Hayashi, T. Kaito, S. Ohtsuka, H. Masuda, S. Taniguchi, E. Sato, J. Nucl. Mater. 466 (2015) 653–657.
[13] C. Herring, J. Appl. Phys. 21 (1950) 437.
[14] R.L. Coble, J. Appl. Phys. 34 (1963) 1679.